SCIENTIFIC PAPERS
OF THE UNIVERSITY OF PARDUBICE
Series A
Faculty of Chemical Technology
5 (1999)

INFLUENCE OF THE FLUIDIZED BED FLOW REGIME ON THE PERMEATE FLUX IN CERAMIC MEMBRANE MICROFILTRATION

Petr MIKULÁŠEK
Department of Chemical Engineering, University of Pardubice,
CZ-532 10 Pardubice

Received October 22, 1999

The influence of a fluidized bed on permeate flux during the microfiltration of model dispersions on ceramic membranes has been studied. Following the description of the basic characteristic zirconium dioxide tubular membranes, model dispersions and spherical particles used, some comments about the experimental system, and experimental results for different microfiltration systems are presented. From analysis of experimental results it may be concluded that the use of a fluidized bed resulted in a significant increase of permeate flux in comparison with results obtained in an empty tube system. This phenomenon is especially pronounced during the microfiltration of oil emulsion when the permeate flux in a fluidized bed system was nearly three times higher. Then, it was found that the optimum porosity of a fluidized bed during which maximal values of permeate flux were reached is in an interval around the value of 0.8. Experimental observations of the onset of aggregate (bubbling) behaviour in liquid fluidized beds are shown to agree with the predictions of a recently published model of the fluidization process. For a given liquid, the transition from particulate to aggregate fluidization depends on both the density and size of the fluidized particles

Introduction

Microfiltration is the pressure-driven membrane process which most closely resembles conventional coarse filtration. The pore sizes of microfiltration membranes range from 10 to 0.05 μm, making the process suitable for retaining suspensions and emulsions. The process is applicable for the water and wastewater treatment processes, the processing of food and dairy products, the recovery of electrodeposition paints, the treatment of oil and latex dispersions and in biotechnology and biomedical technology. In biotechnology, microfiltration is especially suitable in cell harvesting and as a part of membrane bioreactor (involving a combination of biological conversion and separation). However, the present membrane processes for liquid feed streams are complicated by the phenomena of membrane fouling and of concentration polarization in the liquid boundary layer adjacent to the membrane wall. Concentration polarization and membrane fouling are major concerns for the successful use of membrane-based separation operation in a cross-flow mode, as their net effect is to reduce the permeate flux, thereby resulting in a lower productivity. Such limitations have spurred research into the development of new membrane materials and the utilization of novel hydrodynamic approaches in membrane separation systems.

The use of inorganic membranes in separation technologies is relatively new and has given rise to much of interest over recent years. The main group of ceramics used in ceramic-membrane manufacturing are the refractory oxides: alumina, zirconia and titania. Ceramic membranes offer excellent chemical, thermal, and pressure resistance to a wide variety of feed conditions which are only partially developed with (or are completely absent from) polymeric membranes. For example, ceramics can be used at significantly higher temperatures, have better structural stability without the problems of swelling or compaction, can usually withstand harsher chemical environments, are not subject to microbiological attack, and can be backflushed, steam sterilised or autoclaved. Ceramic membranes represent a distinct class of inorganic membranes. Other classes include membrane materials such as glasses, carbon and metals, and organic-inorganic polymers [1].

A number of techniques can be employed to enhance flux rate and minimise fouling in microfiltration by maximising mass transfer at the surface of the membrane. Of the various methods mentioned in Ref. [2], hydrodynamics or fluid management techniques have proved to be quite effective and economical in reducing concentration polarization and fouling. Each of these methods achieved certain success in practice. For example it was reported that membrane systems with fluidized bed in retentate have been used successfully to liquid food processing (see Refs [3–6]).

The fluidized bed concept needs to operate with tubular membrane modules in vertical position. The principle of intensifying mass transfer and a significant reduction of concentration polarization is mainly based on the effect on the

membrane wall caused by the collision of fluidized particles (polymer, metal or glass balls). This interaction reduces, in comparison with the empty tube experiments, the thickness of the boundary layer and increases the mass transfer coefficient [4,6–8].

In the papers [9,10], more closely focused on cross-flow microfiltration of latex waste water on aluminium oxide membranes, we demonstrated that a limiting flux was observed which depended on the types of the latexes and on the flow velocity of the feed. The decrease in the flux of permeate was attributed to the resistance of the cake (gel) layer formed on the membrane or blocking of the pores in the membrane. Therefore, low permeate fluxes resulted at relatively high solution velocity.

In the present study ceramic membrane microfiltration of model dispersions with a fluidized bed in retentate has been studied in some detail. The effects of the superficial velocity and porosity of fluidized bed on the permeate flux are discussed. Attempts have also been made to explain basic transport mechanisms that take place at the wall of membranes from movements of free spherical particles and the systematic evaluation of the effect of particle properties on the observed behaviour of microfiltration systems in the presence of a fluidized bed.

Experimental

Membranes

The membranes used were asymmetric, three layered, internal-pressure-type ceramic microfiltration membranes supplied by Membralox (France). They were configured as single cylindrical tubes 0.2 m long, with an inside diameter of 7 mm, and outside diameter of 10 mm, consisting of a thin zirconium dioxide layer deposited on the internal surface of the tubular aluminium oxide support. In our experiments microfiltration membranes were used with the mean pore diameter equal to 0.1 μm. The membrane pore size distribution was determined by the liquid displacement method [11]. The data presented in Fig. 1 indicate that the ceramic membrane used in these studies has a very narrow pore size distribution.

Feeds

Two different kinds of feed were used either with the empty tube or the fluidized bed system to determine the effect on flux. The first one was the commercial metal-working oil emulsion ERO-SB (Paramo Pardubice, Czech Republic) with mean particle diameter equal to 0.150 μm and the second one was commercial pigment

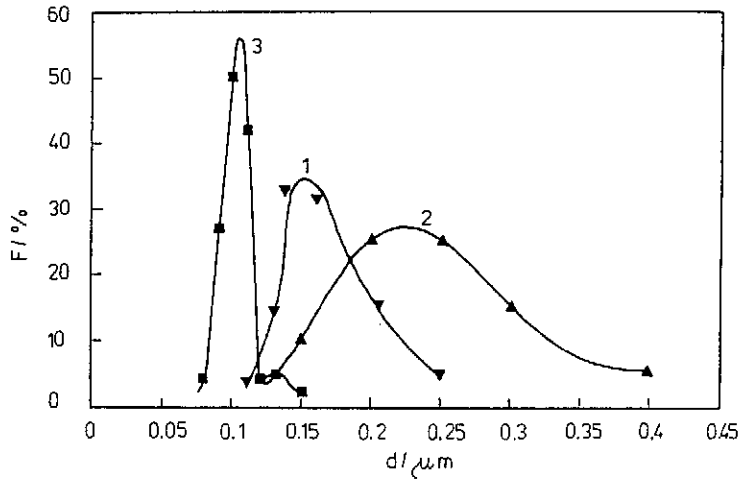

Fig. 1 Particle size distribution of oil emulsion (1), pigment dispersion (2), and pore size distribution of 0.1 μm membrane used (3)

dispersion (white Versanyl, Ostacolor Pardubice, the Czech Republic) with mean particle diameter equal to 0.265 μm. The particle size distributions of the dispersions used, shown in Fig. 1, were determined with the help of a particle sizer BI-90 (Brookhaven Instr. Corp.). Concentration of solids in the dispersions was 0.5% (w/w) for the oil emulsion, and 1% (w/w) for the pigment dispersion.

Equipment

The microfiltration studies were carried out in a membrane filtration unit equipped with ceramic membranes. The unit contained two identical modules: one with fluidized bed in retentate and second with an empty membrane. The fluids were circulated through the module by means of centrifugal pump. The unit allowed studies in which the transmembrane pressure and the cross-flow velocity were independently varied. A schematic diagram of the experimental apparatus is shown in Fig. 2. It consisted mainly of a microfiltration module (1), a pump (2), a storage tank (3) equipped with a thermal regulation system (4), and a temperature and pressure control system.

Experiments were carried out at 20 °C, either with (fluidized bed experiments) or without (empty tube experiments) particles. The liquid was fed into the bottom of the vertical membrane at a constant volumetric flow rate regulated with control valves located at the pump outlet. The supports of the membrane consist of two stainless steel meshes compressed between rubber packing. A cal-

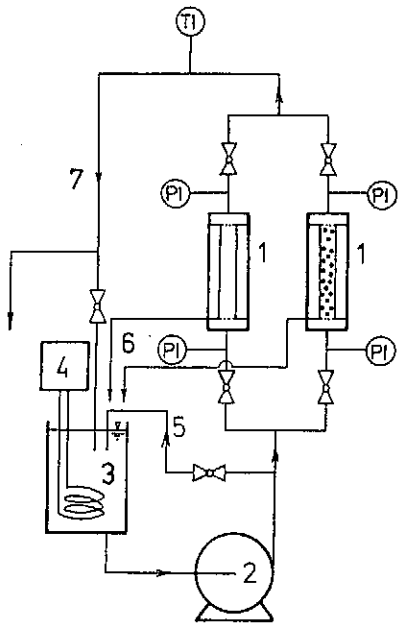

Fig. 2 Scheme of experimental apparatus: 1 – microfiltration module; 2 – pump; 3 – storage tank; 4 – thermal regulating system; 5 – by-pass; 6 – permeate outflow; 7 – retentate outflow

ming section of 2 mm diameter spheres was placed immediately below the support.

At first, the flow of prefiltered deionized water through the membrane was examined under various transmembrane pressures (i.e., the difference between values of the pressures measured by means of two pressure gauges PI and permeate outlet pressure — see Fig. 2) in the range of 0 – 200 kPa, while the superficial velocity was fixed at a constant value. (It is worth recalling that superficial velocity, u, is defined in both the systems as the ratio of volumetric flow rate to membrane tube cross-sectional area). Then, the dispersion was measured at a constant transmembrane pressure ΔP = 200 kPa. For various superficial velocities in the range of 0.025 – 0.25 m s^{-1}, the permeate flux, J, was evaluated. The contribution to the transmebrane pressure drop due to the fluid flow through the fluidized bed resulted in a pressure drop of 2 kPa. Thus, at a total transmembrane pressure of 200 kPa, the pressure drop attributable to the fluidized bed was only 1%, hence the fluidized bed pressure drop was assumed to be negligible for all calculations. A new membrane was used in each experiment, and the pure water flux through the membrane was measured before each run. The dispersion was then introduced to the unit, the pump was powered on and operating pressure and superficial velocity adjusted by the regulation system. The flux through the membrane was measured by

collecting the permeate from the outer Perspex tube surrounding the membrane into graduated cylinder and timing the collection period. Both the permeate and the retentate were recycled to the storage tank to maintain a relatively constant dispersion concentration. Every experiment was carried out until the flux became actually constant.

The fluidized particles were either glass beads (1.465 mm diameter, 2506 $kg\,m^{-3}$ density) or stainless steel beads (0.635, 0.800, and 1.000 mm diameters, 7506 $kg\,m^{-3}$ density). For each experiment with fluidized bed, the column was filled with solids in such a way that the total expanded bed height was equal to membrane length. The corresponding solid loading and superficial velocities were known from preliminary results on hydrodynamics obtained in a transparent tube with the same diameter as the membrane.

Results and Discussion

Microfiltration of model dispersions

Oil emulsion

Analysis of the permeate composition showed complete absence of the dispersion particles from the retentate. Note that for all experimental runs the diameter of the dispersion particles was always larger than the membrane pore size (see Fig. 1) in order to prevent particle penetration into or through the membrane.

Values of permeate flux versus time for various mean feed velocities in the empty tube system are plotted in Fig. 3 for the oil emulsion used. As a general rule, the steady-state flux during cross-flow microfiltration was substantially lower than the pure water flux — ranging from 5% to 12.5% of the pure water values. Beside the fact that high levels of permeate flux are achievable, the most noticeable feature in Fig. 3 is the strong dependence of the flux on the superficial velocity of the feed. The following trends are evident:

a) A significant flux decline was observed mainly in the initial periods of the process,

and

b) the flux decline shows significant dependence on operating conditions such a superficial velocity.

The flux decline in the initial periods of process could be explained by the formation of concentration polarization and/or a gel layer on the membrane surface which offers the controlling hydraulic resistance to permeation. Steady-state conditions as a result of concentration polarization are reached when the convective transport of particles to the membrane is equal to the sum of the permeate flow plus the diffusive back transport of the particle. (It should be remembered that only con-

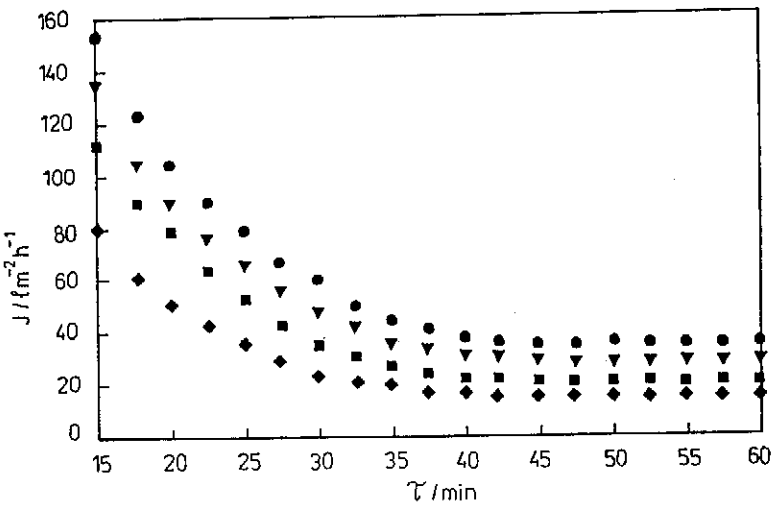

Fig. 3 Permeate flux vs. time for oil emulsion microfiltration — empty tube experiments: ◆ $u = 0.025$ m s^{-1}; ■ $u = 0.065$ m s^{-1}; ▼ $u = 0.150$ m s^{-1}; ● $u = 0.230$ m s^{-1}. (concentration of solids in the dispersion 0.5 % (w/w), transmembrane pressure 200 kPa)

centration polarization phenomena are considered here with fouling being excluded). It is evident from Fig 3. that the steady-state flux increases (the thickness of the concentration polarization layer and its hydraulic resistance decreases) with the superficial velocity.

Figure 4 illustrates the effect of the shear rate at the inner membrane surface on the steady-state permeate flux, J_{SS}, (in a log-log scale) for the oil emulsion sample. The shear rate, assuming Newtonian fluid behaviour of the oil emulsion and fully-developed laminar flow, was approximated for the cross-flow tube system by Eq. (1)

$$\gamma = \frac{8u}{D} \tag{1}$$

substituting the corresponding experimental values of superficial velocity, u.

The slope of the plot is 0.35, which is very close to the one-third power dependency of a system operating under laminar conditions and predicted by the Brownian diffusion mechanism of concentration polarization [12].

To evaluate the possible mechanisms of the flux decline, we have also considered the rinsing behaviour of ceramic microfiltration membranes after their exposure to the dispersions [10]. In experimental terms, irreversible membrane fouling represents the decrease in flux (compared with the original pure water flux)

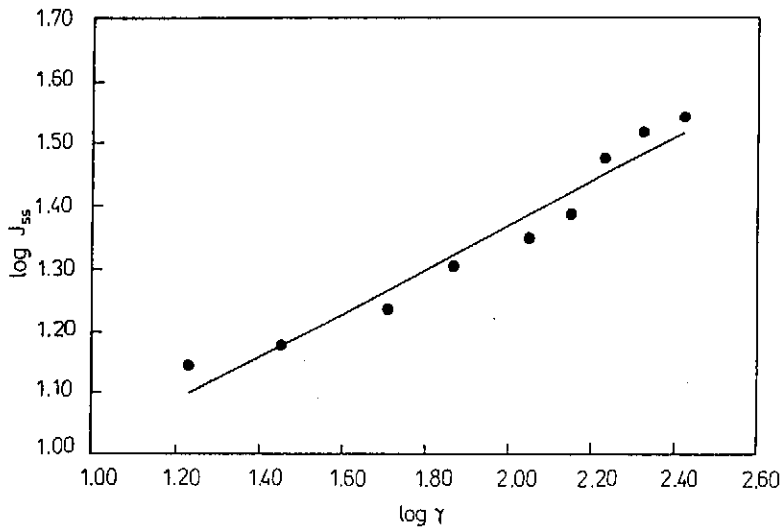

Fig. 4 Steady-state permeate flux vs. shear rate for oil emulsion microfiltration — empty tube experiments. (concentration of solids in the dispersion 0.5 % (w/w), transmembrane pressure 200 kPa)

observed when the feed stream is replaced by pure water, supposedly leaving the irreversible fouling deposit intact. The flux increased quickly with rinsing, then flattened out and appeared to asymptotically approach a final value after 30 minutes. The value of rinsing flux reached up to 90% of the pure water flux, indicating low irreversible fouling for the oil emulsion. This could be attributed to dominant concentration polarization near the ceramic membrane surface.

The values of permeate flux versus time show in the course of microfiltration in the presence of fluidized particles the same shape of $J(\tau)$ curves as compared with those of the empty tube experiment (see Fig. 3). However, a strong and non-monotonous dependence of permeate flux at steady-state, J_{SS}, upon the superficial fluid velocity and/or porosity may be observed. As a rule, the values of the steady-state permeate flux in the fluidized bed system are superior to the ones obtained in the empty tube, with a maximum ratio equal to 2.7.

From Fig. 5 it can be seen a strong dependence of the steady-state flux on particle diameters and the porosity of the bed. The permeate flux through the membrane increases with decreasing particle diameters. Glass beads (1.465 mm diameter) have very small intensification effect on the permeate flux, while the use of steel particles resulted in a significant increase in the permeate flux through the membrane. The density of the glass particles is too low to erode concentration polarization layer on the membrane surface, which results in a very small increase of the permeate flux.

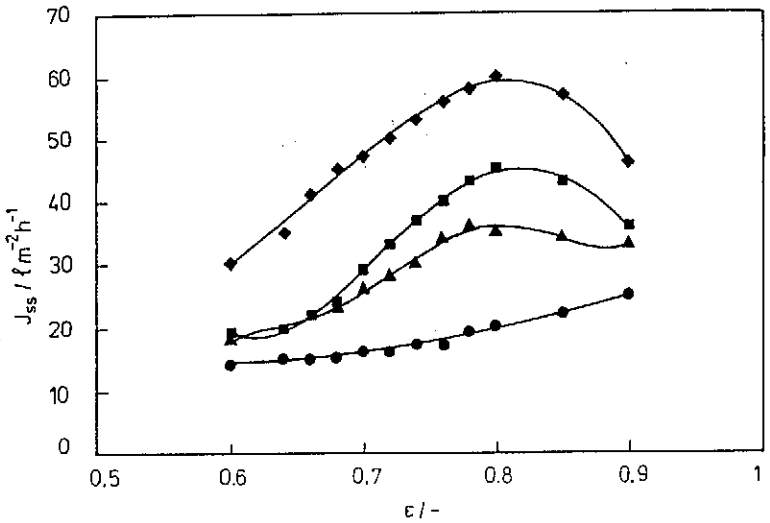

Fig. 5 Variation of steady-state permeate fluxes with fluidized bed porosity for oil emulsion microfiltration: ◆ steel beads d_p = 0.635 mm; ■ steel beads d_p = 0.800 mm; ▲ steel beads d_p = 1.000 mm; ● glass beads d_p = 1.465 mm. (concentration of solids in the dispersion 0.5 % (w/w), transmembrane pressure 200 kPa)

Pigment dispersion

The experiments showed similar time dependence of the flux decline in the empty tube experiments for a pigment dispersion as in the experiments with the oil emulsion: the steady-state flux is lower than the pure water flux. In contrast to the oil emulsion experiments, the formation of a cake layer on the membrane surface together with membrane fouling are dominant.

Similar conclusions as for the oil emulsion can be derived from the fluidized bed experiments: the fluidized bed values for the steady-state permeate flux are higher than those obtained in the empty tube system. However, the maximum ratio is lower when compared with oil emulsion experiments (it is about 1.7 for a pigment dispersion).

Figure 6 shows dependency of the steady-state permeate flux on the porosity of the bed for a pigment dispersion microfiltration. This plot is similar to that obtained for the oil emulsion. From Fig. 6 it can be seen that even the glass particles have considerable intensification effect on the permeate flux (1.3 fold increase). The porosity values for maximum steady-state permeate flux correspond to the theoretical values of the critical porosity even better than in the oil emulsion experiments.

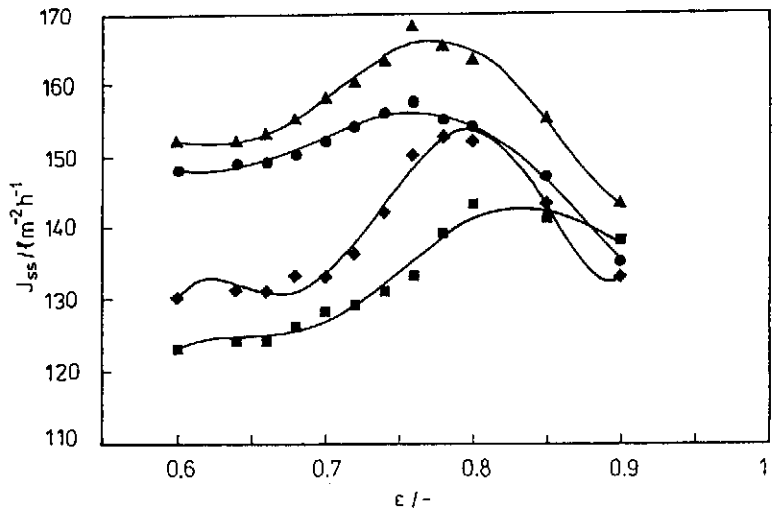

Fig. 6 Variation of steady-state permeate fluxes with fluidized bed porosity for pigment dispersion microfiltration: ◆ steel beads d_p = 0.635 mm; ■ steel beads d_p = 0.800 mm; ▲ steel beads d_p = 1.000 mm; ● glass beads d_p = 1.465 mm. (concentration of solids in the dispersion 1% (w/w), transmembrane pressure 200 kPa)

On the whole, these results agree well with the scattered information on the intensification of microfiltration by a fluidized bed already published in literature [5,6,8]. Solids act as obstacles to the fluid flow in the same way as if they were fixed within a membrane: because of their presence, turbulence is increased and concentration polarization is weaker and/or cake layers are considerably thinner than in the empty tube. However, particle motion may be thought of as being responsible for strong and continuous erosion of particle deposits at the wall. The number of collisions of the particles per unit membrane area per unit of time is proportional to bed porosity [4]. Particle-cake contacts are certainly more effective than turbulence when ε is varied in interval around the value of 0.8 (see Fig. 6), where the fluidized bed is less stable, because the bridge-like particle agglomerates are formed, and a slugging flow is observed (see Fig. 7). Particles form layers, or slugs, between the large liquid pockets and tend to move upward in a piston-like manner.

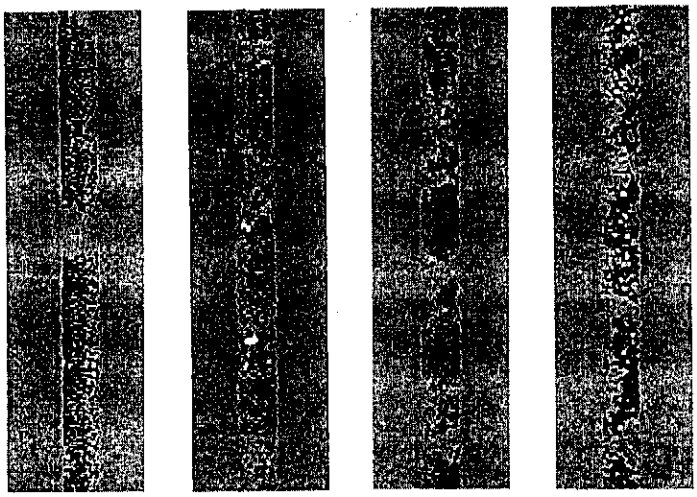

Fig. 7 Slugging flow in a fluidized bed of 1.000 mm steel beads fluidized by ambient water

Stability of a fluidized bed

Further understanding of the erosive action of the particles may be obtained when the results of fluidized bed microfiltration experiments are compared with some visual observations, and the prediction of the stability of a homogeneous fluidized bed. Wallis [13] has shown that the stability of a fluidized bed entirely depends on the relative magnitude of dynamic and continuity wave velocities in the bed. If the dynamic velocity is greater than the continuity wave velocity, the bed will display particulate behaviour, and if the continuity wave velocity exceeds the dynamic wave velocity, inhomogeneous voidage will grow and can develop into complete aggregation. To quantify Wallis stability criterion, Gibilaro *et al.* [14] formulated the following dimensionless expression

$$F_U = \frac{U_e - U_\varepsilon}{U_e} \tag{2}$$

The values of U_e and U_ε can be obtained from the following equations given by Foscolo and Gibilaro [15]

$$U_e = \left[\frac{3.2gd_p(1-\varepsilon)(\rho_p - \rho_l)}{\rho_p}\right]^{0.5} \tag{3}$$

$$U_\varepsilon = nU_t(1-\varepsilon)\varepsilon^{n-1} \tag{4}$$

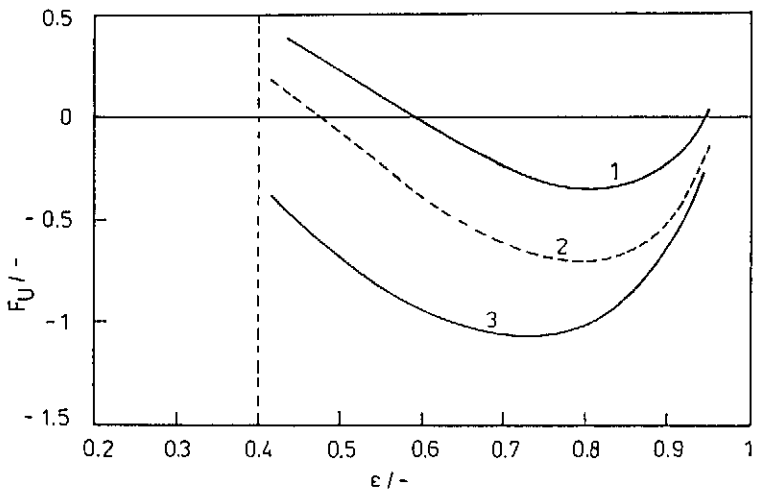

Fig. 8 Effect of particle diameter on the state of aggregation: 1 – steel beads d_p = 0.635 mm; 2 – steel beads d_p = 0.800 mm; 3 – steel beads d_p = 1.000 mm (water, temperature 20 °C)

For a given system (in which the fluid density and viscosity, and particle density and diameter, are specified) F_U may readily be evaluated as a function of voidage: positive and negative values of F_U represent particulate and aggregate types of behaviour, respectively, and a zero value pinpoints the voidage at which a transition from particulate to aggregate fluidization is predicted to occur.

The effect of the individual system variables on bed stability may readily be assessed, permitting systematic studies to be made. This we have now illustrated with the reference to the fluidization of spherical particles by water. The F_U functions for steel particles similar to those used in the present investigation are plotted in Fig. 8 as a function of bed voidage. Two regimes of fluidization can be identified: steel particles below 0.3 mm are fully in the particulate fluidization regime, particles between 0.6 mm and approximately 0.8 mm pass through both regimes and particles larger than 0.9 mm are always in the aggregate regime. For a given F_U value, the bed voidage depends considerably on the particle diameter du-

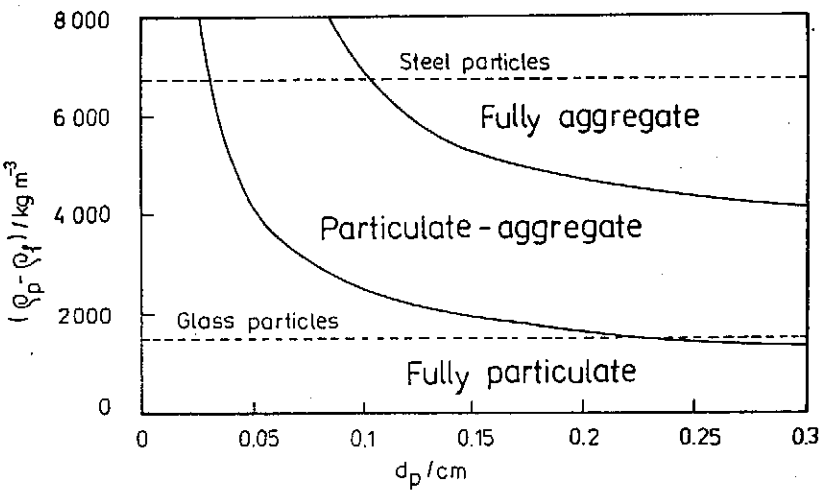

Fig. 9 Particle classification for fluidization by ambient water

ring particulate fluidization or particulate-aggregative fluidization, whereas the effect of particle size (and density) almost disappears with decreasing F_U, when changes occur within the fully aggregate regime. A similar transitional effect was also observed in the experimental results of Hirata and Bulos [16] and correlates well with the transition of fluidization regimes indicated in Fig. 8.

The above model can be used to construct a flow map as shown in Fig. 9. This diagram may be used to predict the effect of physical properties of the solid and liquid phase on the state of aggregation of the fluidized bed.

On the basis of experiments in a transparent tube with the same diameter as the microfiltration membrane it was found that value of the critical bed porosity is close to 0.75 which is slightly lower than the values obtained in fluidized bed microfiltration. These interesting experimental results indirectly confirm the measured trends obtained during microfiltration experiments in the presence of the fluidized bed (see Figs 5 and 6). However, it should be noted that the predictions of the fluidized bed stability are valid for non-porous tube only, and are very sensitive to the particle Reynolds number Re_f, and the density ratio, ρ_p/ρ_f.

Conclusion

The results presented demonstrate that the ceramic microfiltration membranes used are useful for removal or recuperation of oil emulsion and pigment dispersions from wastewater or process streams.

The use of turbulence-promoting fluidized particles resulted in a significant

increase of permeate flux through the membrane. However, it has been noticed that the flux reaches a maximum for the optimum bed porosity in dependence on the superficial velocity of the feed and on the behaviour of the fluidized bed.

From analysis of hydraulic resistances it may be concluded that fluidized solids insure a significant reduction of the concentration polarization as well as a continuous mechanical erosion of the particles deposit at the wall of the membrane. In this case the improved permeate flux that is achieved is due to the combined action of turbulence and particle motion (collision of particles with membrane wall). This reduces the thickness of the surface boundary layer and reduces hydraulic resistance of concentration polarization and/or a cake layer. Thus, the properties, formation, and movement of particles are dominant factors that will determine the overall behaviour of the fluidized bed microfiltration system. The theoretical predictions of the stability of a homogeneous fluidized bed seem to be in good agreement with the experimentally observed results during the cross-flow microfiltration in the presence of a fluidized bed.

Symbols

d diameter of dispersed particles or membrane pores, m
d_p diameter of particle in fluidized bed, m
D inner diameter of the membrane tube, m
F_U dimensionless function, Eq. 2
J permeate flux, $l\,m^{-2}\,h^{-1}$
J_{SS} steady-state permeate flux, $l\,m^{-2}\,h^{-1}$
n exponent in the Richardson-Zaki-type equation
ΔP transmembrane pressure, Pa
u superficial velocity of the feed, $m\,s^{-1}$
U_e elastic wave velocity, $m\,s^{-1}$
U_ε voidage propagation velocity, $m\,s^{-1}$
U_t unhindered particle settling velocity, $m\,s^{-1}$
γ shear rate at wall, s^{-1}
ε bed porosity
ρ_l liquid density, $kg\,m^{-3}$
ρ_p particle density, $kg\,m^{-3}$
τ time, s

References

1. Bhave R.R. *Inorganic Membranes*, p. 10-63, Van Nostrand Reinhold, New York 1991.

2. Mikulášek P.: Coll. Czech. Chem. Commun. **59**, 737 (1994).
3. Van der Waal M.J., Van der Velden P.M., Koning J., Smolders C.A., van Swaay, W.P.M.: Desalination **22**, 465 (1977).
4. De Boer R., Zomerman J.J., Hiddink J., Aufderheyde J., van Swaay W.P.M., Smolders C.A.: J. Food Sci. **45**, 1522 (1980).
5. Montlahuc G., Tarodo de la Fuente B., Rios G.M.: Entropie **124**, 24 (1985).
6. Rios G.M., Rakotoarisoa H., Tarodo de la Fuente B.: J. Membr. Sci. **34**, 331 (1987).
7. Xuesong W.: Desalination **62**, 211 (1987).
8. Clavaguera F., Rjimati E., Elmaleh S., Grasmick A.: Key Eng. Mater. **61/62**, 569 (1991).
9. Mikulášek P., Cakl J.: Desalination **95**, 211 (1994).
10. Cakl J., Mikulášek P.: Sep. Sci. Technol. **30**, 3663 (1995).
11. Mikulášek P., Doleček P.: Sep. Sci. Technol. **29**, 1183 (1994).
12. Belfort G., Davis R.H., Zydney A.L.: J. Membr. Sci. **96**, 1 (1994).
13. Wallis G.B.: *One-Dimensional Two-Phase Flow*, McGraw-Hill, New York 1969.
14. Gibilaro L.G., Hossain I., Foscolo P.U.: Can. J. Chem. Eng. **64**, 931 (1986).
15. Foscolo P.U., Gibilaro L.G.: Chem. Eng. Sci. **39**, 1667 (1984).
16. Hirata A., Bulos F.B.: J. Chem. Eng. Japan **23**, 599 (1990).